https://doi.org/10.5194/egusphere-2026-6504
Preprint. Discussion started: 23 November 2026
© Author(s) 2026. CC BY 4.0 License.

Effects of Particle-Size Distribution on the Charging of Dust in the Mesosphere / Lower Thermosphere

Ingrid Mann[1], Adrien Pineau[2], Isabel Nerland[1], Yoshihiro Yokoyama[1], Herman Greaker[1,3], Aigen Li[4], and Wuhu Feng[5]

[1]Department of Physics of Technology, UiT Artic University of Norway, 9037 Tromsø, Norway
[2]Laboratory for Laser Energetics, University of Rochester, 250 E. River Rd, Rochester, NY, USA
[3]Andøya Space AS, Bleiksveien 46, 8480 Andenes, Norway
[4]University of Missouri, Columbia, MO, USA
[5]National Centre for Atmospheric Science, University of Leeds, Leeds, United Kingdom
[*]**Correspondance:** Ingrid Mann (ingrid.b.mann@uit.no), Yoshihiro Yokoyama (yoshihiro.yokoyama@uit.no)

Abstract.

Small, refractory solid particles are abundant in the mesosphere and lower thermosphere, which overlaps with the D-region of the ionosphere. The vast majority of this dust form from cosmic dust deposited through the meteors. These particles are known as meteoric smoke and they affect the charge balance, physics and chemistry of the ambient medium. It has recently been discussed that material released during satellite launches and spacecraft reentry may constitute an additional anthropogenic source of dust particles in the mesosphere. The electric surface charge of the dust particles is an important factor in determining their interactions and evolution.

We calculate the charge states of solid particles in the mesosphere, accounting for their interactions with photons, atmospheric electrons, and ions. Building on previous studies, we solve the coupled charge-balance equations for a range of particle sizes. In this work, we investigate the effect of the size distribution on the charge of the dust along with dust composition. We consider dust radii of approximately 0.2–50 nm in line with studies describing the evolution of meteoric smoke particles. The description of the dust charging model is however applicable to solid particles down to radii of about 0.8 nm. We kept smaller sizes in the model for illustration but their charge contribution was negligible. Although the qualitative behavior of the distributions of positively charged, negatively charged, and neutral dust particles remained unchanged, the calculated number of charged dust changed by up to a factor of three when the size distribution was taken into account. We find that positively and negatively charged particles coexist and are often present in comparable abundances. Positive charge states become more abundant at larger dust sizes, whereas negative charge states dominate among the smallest dust particles. Most sub-nanometer dust particles are neutral, although a small fraction remains negatively charged even at the smallest sizes considered. While the charging framework includes charge states up to ± 3, the triple charge states are negligible and the double charge state only plays a role for the size distribution with relatively large amount of large particles. A further notable result related to the planning and analysis of in-situ measurements is that the change of the net charge density of dust with height is more pronounced than the differences in charge density on the dust due to composition.

https://doi.org/10.5194/egusphere-2026-6504
Preprint. Discussion started: 23 November 2026
© Author(s) 2026. CC BY 4.0 License.

1 Introduction

Small solid particles in the mesosphere–lower thermosphere (MLT) are believed to form from remnants of cosmic dust entering Earth's atmosphere. Cosmic dust particles of certain sizes and velocities vaporize when entering the Earth atmosphere, give rise to meteor phenomena and release dust material in the ambient medium, that is the MLT and the overlapping D-region ionosphere. The cosmic material condenses into solid particles, denoted as meteoric smoke particles, MSP. The MSP grow upon mutual collisions, influenced by atmospheric winds and turbulence, and gravitational settling. These processes have been studied thanks to the developments allowing including the MSP into global simulation frameworks (Megner et al., 2008b; Bardeen et al., 2008). The MSP participate in ionospheric charging processes (Baumann et al., 2013), thereby affecting ion chemistry (Plane et al., 2015). This topic gains further importance because space debris deposited in the atmosphere provides an additional and increasing source for the formation of solid dust in the MLT (Schulz et al., 2026). Metals from spacecraft reentry have been found in stratospheric aerosol particles (Murphy et al., 2023) and this motivated the discussion of anthropogenic smoke particles (ASP) (Sana et al., 2026) being present in the MLT.

The dust particles may also take part in the formation of ice particles (Rapp and Thomas, 2006) that form polar mesospheric clouds (Hervig et al., 2001), often denoted as noctilucent clouds (NLCs) when observed from the ground. The abundance of these clouds is increasing over the last decades hereby changing the solar UV absorption in the upper atmosphere (Luebken et al., 2023). Although it has often been discussed that MSPs are the particles enabling the heterogeneous condensation that leads to the formation of NLCs, simulations led to MSP concentrations that seem be too low for this (Megner et al., 2008a). Studies with improved condensation models have confirmed the necessity of heterogeneous condensation (Tanaka et al., 2022). The charge of condensation nuclei was not included yet in the study, although it also plays a role (Rapp and Thomas, 2006; Gumbel and Megner, 2009; Megner and Gumbel, 2009). The charge effects have been recently studies for coalescence of particles including also the like-charge attraction (Baptiste et al., 2020; Sana et al., 2026). As the charge of MSP affects the ionospheric charge balance, it is possibly observed with the radar studies of the D-region ionosphere based on incoherent scatter process (Gunnarsdottir et al., 2023). Furthermore, the charge of dust particles is an important parameter for analyzing measurement with rocket-borne instruments that are based or partly based on the detection of electric charge (Antonsen et al., 2017).

Dust particles with sub-micrometer sizes become electrically charged in the D-region of the ionosphere through the accumulation of plasma particles. This charging process is governed by the thermal motion of the plasma, Coulomb forces, and polarization-induced image forces between the sub-micrometer particles and the plasma ions and electrons. Natanson (1960) described the charging process of a sub-micrometer particle in a plasma using gas-kinetic theory, with the plasma particles treated as point charges and derived an expression for their capture rate by dust particles. While the full description of the capture rate generally requires numerical evaluation, he also proposed an analytical approximation. Rapp (2000) demonstrated the applicability of this analytical description under mesopause conditions, and it has been widely used ever since. Notably, also photo ionization and photo detachment have been included as additional processes (Rapp, 2009). The dust charging was investigated for the case of the polar summer mesosphere with a set of charging rates including the collisions with the iono-

https://doi.org/10.5194/egusphere-2026-6504
Preprint. Discussion started: 23 November 2026
© Author(s) 2026. CC BY 4.0 License.

spheric particles as well as photoemission and photodetachment rates (Knappmiller et al., 2011; Asmus et al., 2015). These simulations consider individual MSPs undergoing charging processes in the ionosphere and eventually reaching an equilibrium charge. However, they neglect the influence of MSP particles on the ionospheric charge carriers and, consequently, on the charging of other MSPs. In this work, we develop a system of coupled rate equations to simulate the charging of MSPs with a size distribution.

The remainder of the manuscript is structured as follows. In the next section (section 2), we introduce the charging equations, the dust-material parameters used to determine the relevant charging parameters, and the two size distributions of MSPs considered in this study. We apply this system to summer conditions in the MLT region at high latitudes and obtain charge distributions as function of height for different MSP conditions and present the results in section 3. The results are summarized in section 4 and supporting information is given in the appendix.

https://doi.org/10.5194/egusphere-2026-6504
Preprint. Discussion started: 23 November 2026
© Author(s) 2026. CC BY 4.0 License.

2 Model description

2.1 MSP charging dynamics

To evaluate the charge distribution of MSP in the upper atmosphere, we consider the following processes: (i) electron attachment where a free electron is captured at the MSP surface, (ii) ion attachment where a free ion is captured at the MSP surface (iii) photo-ionization where a solar photon is absorbed by a MSP generating a free electron, and (iv) photo-detachment where a solar photon is absorbed by an electron attached to the MSP surface releasing it. The dynamics associated with these processes is schematically illustrated in Figure 1. We assume that MSP can not carry more than 2 charges leading to a set of five possible ionization states $Z \in \{-2,-1,0,+1,+2\}$. We will show later that densities for MSP with $Z \leq -3$ or $Z \geq +3$ are negligible. When an ion is captured by an MSP already carrying one or two electrons, the ion can be attached to MSP in addition to the electrons or the ion can recombine with an electron which is lost by the MSP. In both cases, the charge balance is the same since (i) the net charge of the MSP changes from Z to $Z+1$, the ion density decreases because an is captured or recombines, and the electron density remains unchanged because the electron stays on the MSP or recombines. Similarly, an electron can be captured by an MSP carrying one or two ions leading to electron attachment or recombination. In the case of electron or ion attachments, charges can pile up on the MSP which could carry, for instance, 4 electrons and 3 ions with a net charge $Z=-1$ and it would be necessary to consider many cases associated with $Z \in \{-2,-1,0,+1,+2\}$. We assume that in such cases recombination occurs. Regarding processes that involve photons, it can be noted that photo-detachment only happens for MSP carrying electrons. We neglect photo-ionization for MSP with $Z=+1$ as it would be associated with a very high energy bandgap. The densities of MSP with radius r and ionization state $Z \in \{-2,-1,0,+1,+2\}$ are denoted n^{++}_{MSP}, n^{+}_{MSP}, $n^{\emptyset}_{MSP}$, n^{-}_{MSP},

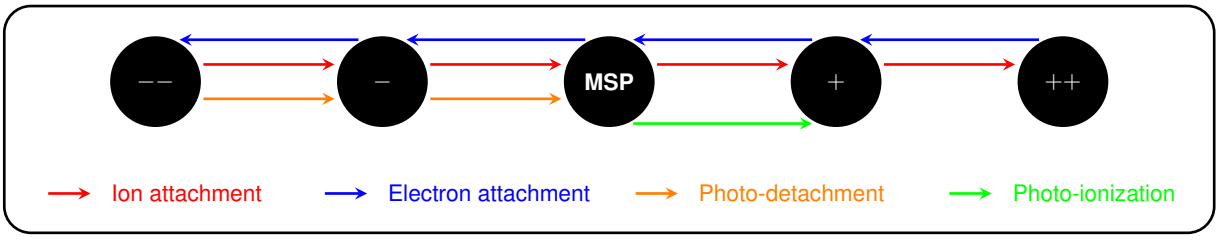


Figure 1. Schematic diagram of the dust particles charging processes

https://doi.org/10.5194/egusphere-2026-6504
Preprint. Discussion started: 23 November 2026
© Author(s) 2026. CC BY 4.0 License.

and n_{MSP}^{--} respectively. They are evaluated with a set of coupled rate equations:

$$\frac{dn_{MSP}^{--}}{dt} = \alpha_{EA}(Z=-1)\,n_{MSP}^{-}n_e - \alpha_{IA}(Z=-2)\,n_{MSP}^{--}n_i - \beta_{PD}(Z=-2)n_{MSP}^{--} \tag{1}$$

$$\begin{aligned}\frac{dn_{MSP}^{-}}{dt} = &-\alpha_{EA}(Z=-1)\,n_{MSP}^{-}n_e + \alpha_{IA}(Z=-2)\,n_{MSP}^{--}n_i + \beta_{PD}(Z=-2)n_{MSP}^{--}\\ &+\alpha_{EA}(Z=0)\,n_{MSP}^{\emptyset}n_e - \alpha_{IA}(Z=-1)\,n_{MSP}^{-}n_i - \beta_{PD}(Z=-1)n_{MSP}^{-}\end{aligned} \tag{2}$$

$$\begin{aligned}\frac{dn_{MSP}^{\emptyset}}{dt} = &-\alpha_{EA}(Z=0)\,n_{MSP}^{\emptyset}n_e + \alpha_{IA}(Z=-1)\,n_{MSP}^{-}n_i + \beta_{PD}(Z=-1)n_{MSP}^{-}\\ &+\alpha_{EA}(Z=1)\,n_{MSP}^{+}n_e - \alpha_{IA}(Z=0)\,n_{MSP}^{\emptyset}n_i - \beta_{PI}(Z=0)n_{MSP}^{\emptyset}\end{aligned} \tag{3}$$

$$\begin{aligned}\frac{dn_{MSP}^{+}}{dt} = &-\alpha_{EA}(Z=1)\,n_{MSP}^{+}n_e + \alpha_{IA}(Z=0)\,n_{MSP}^{\emptyset}n_i + \beta_{PI}(Z=0)n_{MSP}^{\emptyset}\\ &+\alpha_{EA}(Z=2)\,n_{MSP}^{++}n_e - \alpha_{IA}(Z=1)\,n_{MSP}^{+}n_i\end{aligned} \tag{4}$$

$$\frac{dn_{MSP}^{++}}{dt} = -\alpha_{EA}(Z=2)\,n_{MSP}^{++}n_e + \alpha_{IA}(Z=1)\,n_{MSP}^{+}n_i \tag{5}$$

where α_{EA}, α_{IA}, β_{PI}, and β_{PD} are the rates of electron attachment, ion attachment, photo-ionization, and photo-detachment respectively; n_e and n_i are the number densities of free electrons and ions respectively. All rates and densities in the equations above depend on the MSP radius that has been omitted for the sake of clarity. Electron attachment and ion attachment are the results of the Coulomb interaction and the induced polarization interaction taking place between a MSP and a free charge (electron or ion). The expression of the capture rate can be derived by using gas kinetics theory (Natanson, 1960) but it can be simplified in our case since the mean free path is much larger than MSP typical size. In that case, different expressions are obtained whether the net interaction is attractive (electron with a positive MSP or ion with a negative MSP), neutral (that is electron or ion with a neutral MSP), or repulsive (electron with a negative MSP or ion with a positive MSP). We then have (Rapp, 2000) e.g. :

$$\alpha_{EC}(Z>0,r) = \alpha_{IC}(Z<0,r) = \pi r^2 c_s\left(1+\frac{16}{81}\frac{\lambda_{mfp}|Z|e^2}{r\lambda_{mfp}k_BT}\right) \tag{6}$$

$$\alpha_{EC}(Z=0,r) = \alpha_{IC}(Z=0,r) = \pi r^2 c_s \gamma(r)\left(1+\sqrt{\frac{\pi e^2}{2rk_BT}}\right) \tag{7}$$

$$\alpha_{EC}(Z<0,r) = \alpha_{IC}(Z>0,r) = \pi r^2 g^2 c_s \exp\left[-\frac{|Z|^2}{grk_BT}\left(1-\frac{1}{2g\left(g^2-1\right)|Z|}\right)\right] \tag{8}$$

with λ_{mfp} the mean free path of the free charge, e the elementary charge, k_B the Boltzmann constant, T the electron or ion kinetic temperature. Finally, g is a dimensionless factor defined by the distance where the repulsive interaction and attractive interaction cancel each other :

$$|Z| = \frac{2g^2-1}{g\left(g^2-1\right)^2}. \tag{9}$$

We can note that attractive and repulsive interactions are modeled in the same way for electrons and ions, and the only difference lies in the speed of sound $c_{s,e/i} = \sqrt{8k_BT/\pi m_{e/i}}$, with k_B the Boltzmann constant and T the charge components temperature,

https://doi.org/10.5194/egusphere-2026-6504
Preprint. Discussion started: 23 November 2026
© Author(s) 2026. CC BY 4.0 License.

involving the electron mass m_e or the ion mass m_i. The rates for electron attachment and ion attachment are calculated in this work for a temperature $T = 200$ K and ion mass $m_i \simeq 30$ amu as an average value. The photo-ionization rate $\beta_{PI}(Z)$ and photo-detachment rate $\beta_{PD}(Z)$ are calculated similarly by (Nerland, 2024):

$$\beta(Z,r) = \frac{1}{hc} \int_0^{hc/E} \lambda I(\lambda) \sigma(\lambda,r) Y(\lambda) \, \mathrm{d}\lambda \tag{10}$$

where h is the Planck constant, c is the speed of light, E is the cut-off energy, I is the solar irradiance, Y is the quantum yield and $\sigma(\lambda,r)$ is the absorption cross section of the dust particle. Y is the quantum yield corresponding to the probability of an electron ejection following a photon impact assumed to be equal to unity for all wavelengths.

Finally, the charge balance ensuring quasi-neutrality reads :

$$\frac{dn_e}{dt} = Q - \nu_r n_e n_i + \sum_{r=r_{min}}^{r=r_{max}} \left(\sum_{Z=-2}^{Z=+1} n_e \alpha_{EA}(Z,r) n_{MSP}(Z,r) + \sum_{Z=-2}^{Z=-1} \beta_{PD}(Z,r) n_{MSP}(Z,r) + \beta_{PI}(Z=0,r) n_{MSP}(Z=0,r) \right) \tag{11}$$

$$\frac{dn_i}{dt} = Q - \nu_r n_e n_i + \sum_{r=r_{min}}^{r=r_{max}} \sum_{Z=-1}^{Z=+2} n_i \alpha_{IA}(Z,r) n_{MSP}(Z,r) \tag{12}$$

where Q is the electron-ion pair production rate and ν_r is the electron-ion pair recombination rate. We use in this work $Q = 10\ \mathrm{cm}^{-3}.\mathrm{s}^{-1}$ and $\nu_r = 10^{-6}\ \mathrm{cm}^3\mathrm{s}^{-1}$ as mean values. The first, second and third term in the sum over the radii of Equation (11) correspond to electron attachment, photo-detachment, and photo-ionization respectively while the term in the sum over the radii of Equation (12) corresponds to ion attachment. Unlike previous studies using this approach (Knappmiller et al., 2011; Asmus et al., 2015; Nerland, 2024), we here directly consider all MSP sizes lying between minimum radius r_{min} and maximum radius r_{max}; their number densities are described by two different MSP size distributions discussed below. obtained from the LSP GSFC Composite Solar Spectral Irradiance (SSI_3) spectrum, see Nerland (2024) for more information.

From the results obtained by solving the coupled equations, we can sum the charge distribution over the radii:

$$n_{MSP}(Z) = \sum_{r=r_{min}}^{r_{max}} n_{MSP}(Z,r) \tag{13}$$

to obtain the total number density of dust particles associated with each ionization state.

And we can obtain the total charge density as function of height as

$$Q(z) = \sum_{Z=-1}^{1} \sum_{r=r_{min}}^{r_{max}} Z e n_{MSP}(r,Z,z) \tag{14}$$

with e the elementary charge. In a next step we discuss the assumptions for parameters that depends on the MSP composition and the size distributions to be used for the model calculations.

2.2 MSP parameters related to composition

The photo-ionization and photo-detachment rates that determine the charging depend on MSP composition and size. The absorption cross section $\sigma(\lambda,r)$ depends on the optical constants of the MSP material as well as MSP size. In addition, the

https://doi.org/10.5194/egusphere-2026-6504
Preprint. Discussion started: 23 November 2026
© Author(s) 2026. CC BY 4.0 License.

energy thresholds of the photon processes depend on the material. The composition of meteoric smoke particles (MSPs) has not yet been directly determined and the materials discusses which we consider include the magnesium/ion silicates olivine and pyroxene as well as the iron oxides: wüstite, magnesio-wüstite and hematite. Laboratory studies identified hematite as a promising candidate (Saunders and Plane, 2006) and its existence in the upper atmosphere at 60 km has been inferred from observations (Bohren and Olivero, 1984). Satellite observations of polar mesospheric clouds have been explained by the presence of water-ice particles containing small amounts of MSPs composed of carbon, wüstite (FeO), or magnesiowüstite (Hervig et al., 2012). Based on rocket-borne in situ measurements, Rapp et al. (2012) suggested that MSPs are composed of Fe- and Mg-hydroxide clusters. Also iron-rich olivine was discussed as MSP material (Rapp et al., 2010; Hervig et al., 2012).

The MSP absorption cross section $\sigma(\lambda, r) = \pi r^2 Q_{abs}(\lambda, r)$ is deduced from the normalized absorption cross section Q_{abs} that is calculated from the Mie theory and depends on the refractive index of the MSP material (Nerland, 2024). The difference between photo-ionization and photo-detachment lies in the upper limit of the integral where the energy depends on the photonic process. The cut-off energy corresponds to the work function for photo-ionization and to the electron affinity for photo-detachment. They depend on the MSP material composition which little is known about.

To describe the photo-ionization the absorption cross-section is calculated using Mie theory describing spherical particles with a given radius and complex refractive index. The indices used are from the data base of the Laboratory Astrophysics Group at University of Jena including parameters published (Henning et al., 1995a; Jäger et al., 1994). The values were interpolated between the values given in the archives. The values for work function and electron affinity were collected from several works listed in Nerland (2024) and given in Table 1. Because the values are uncertain, we use for all cases a value of 5.5 eV for the work function and 2.5 eV for the electron affinity. This approach is also reasonable, because the calculations have shown that most of the difference between the materials is caused by the difference in absorption cross sections.

Table 1. Materials discussed in this work; the wavelength range of optical constants used and the values workfunction, and electron affinity found in the literature. The references given are (a) Henning et al. (1995b), (b) Wang et al. (1996), (c) Rienstra-Kiracofe et al. (2002), (d) **?**, (e) Rapp (2009), (f) Kraushofer et al. (2018), (g) He (2017), (h) Fonin et al. (2005), (i) (Jaeger et al., 1994; Dorschner et al., 1995), and (j) Li et al. (2016).

Material [formula]	**Range of optical constants** (μm)	**Work function** (eV)	**Electron affinity** (eV)
Wüstite FeO	$0.2-500$ (a)	N/A	1.5 (b))
			1.4945 ± 0.0001 (c)
Hematite Fe_2O_3	$0.1-1000$ (d)	5.5 (e)	2.5 ± 0.2 (b)
		5.4 ± 0.2 (f)	3.06 ± 0.04 (c)
		5.49 (g)	
Magnetite $[FeO \cdot Fe_2O_3]$	$0.1-1000$ (d)	5.20 ± 0.15 (h)	2.4 (b)
			2.56 ± 0.06 (c)
Magnesio-wüstite $(Mg,Fe)O$	$0.2-500$ (a)	N/A	N/A
Pyroxene $(Mg,Fe,Ca)SiO_3$	$0.2-10^4$ (i)	5.14 ± 0.36 (j)	N/A
Olivine $Mg_{2x}Fe_{2-2x}SiO_4$	$0.2-10^4$ (i)	7.90 ± 0.35 (j)	N/A

https://doi.org/10.5194/egusphere-2026-6504
Preprint. Discussion started: 23 November 2026
© Author(s) 2026. CC BY 4.0 License.

2.3 Size distribution

There is little direct information on the size distributions of MSP and we therefore use here two very different distributions. We use for one the empirical size distribution suggested by Rapp and Thomas (2006) who compared the different size distributions used and proposed by other authors and noted that these distributions (Hunten et al., 1980; Gabrielli et al., 2004) showed some degree of convergence and could be described by (Rapp and Thomas, 2006) :

$$\frac{dN_{MSP}}{dr} = \eta_0 \exp\left(-\frac{r}{r_0}\right) \tag{15}$$

with $\eta_0 = 4 \times 10^5$ cm^{-3}.nm^{-1} and $r_0 = 0.25$ nm as a reasonable approximation. The size distribution is in this case given by $N(r) = \int_{r_0}^{r} \frac{dN_{MSP}}{dr'} \, dr'$ and we will denote it as the empirical size distribution. The model was assumed also for studies of the MSP affecting the observed extinction in polar mesospheric clouds (Hervig et al., 2021). And this model is in agreement with a power law estimate for MSP radii 0.5 to 1.5 nm (Antonsen et al., 2017) made based on in-situ measurements in a 2016 summer rocket campaign (Antonsen et al., 2017).

As the second MSP particle-size distributions, we use a distribution derived from a WACCM/CARMA three-dimensional model run. WACCM/CARMA was used by Bardeen et al. [2008] to perform a first three-dimensional simulation of meteoric dust in a general circulation model. WACCM is a global circulation climate model that simulates wind patterns and transport processes in Earth's atmosphere using the framework of the Community Earth System Model (CESM). CARMA is a multidimensional microphysics model that tracks and simulates the evolution of meteoric particles. In the coupled model, CARMA calculates the evolution of the constituents using inputs from WACCM. The CARMA results are then passed back to WACCM as constituent fields, modifying the model parameters before the next model iteration.

The dataset used to obtain the particle-size distribution from the Whole Atmosphere Community Climate Model version 4 (WACCM4) (Richter et al., 2008) coupled with the Community Aerosol and Radiation Model (CARMA) (Toon et al., 1979; Turco et al., 1979) (termed as WACCM/CARMA2019). The MSP are divided into 28 radius bins ranging from 0.2 nm to 102.4 nm. The model parameters used in the simulation are those described by Hervig et al. (2021) but used a free running version for 20 years simulations. The MSP density profiles obtained from this model run are discussed by Gunnarsdottir et al. (2023) and Greaker (2023). The size distribution used is derived from the data for the month of July at a location close to Andøya, Norway, 69.9 deg North and 16.2 deg East. We note that this WACCM/CARMA model run produces different MSP profiles in comparison to earlier model runs, which has been discussed in Hervig et al. (2017).

Both size distributions are illustrated in Figure 2 for altitudes of interest located between 70 km and 110 km. The number density height profiles are shown in Figure 3. The empirical distribution is independent of height and we chose the constants so that the total number of dust particles is equal in both models. The empirical distribution predicts a larger amount of small particles, i.e. radii smaller than $\sim$ 1 nm, while the WACCM-CARMA2019 predicts a larger amount of larger particles, i.e. radii larger than $\sim$ 5 nm. Both distributions predict the same number of dust particles for radii of the order of magnitude of $\sim$ 1 nm and altitude higher than 90 km. As larger particles are more influenced by gravity there is a large number of dust particles, with radii from 2 to 10 nm at altitudes lower than 85 km. By merging these size distributions in the set of equations (5)-(1) and (11)-(12), we calculate the charge distribution. The system of equations is solved by using the 4th order Runge-Kutta method over a

https://doi.org/10.5194/egusphere-2026-6504
Preprint. Discussion started: 23 November 2026
© Author(s) 2026. CC BY 4.0 License.

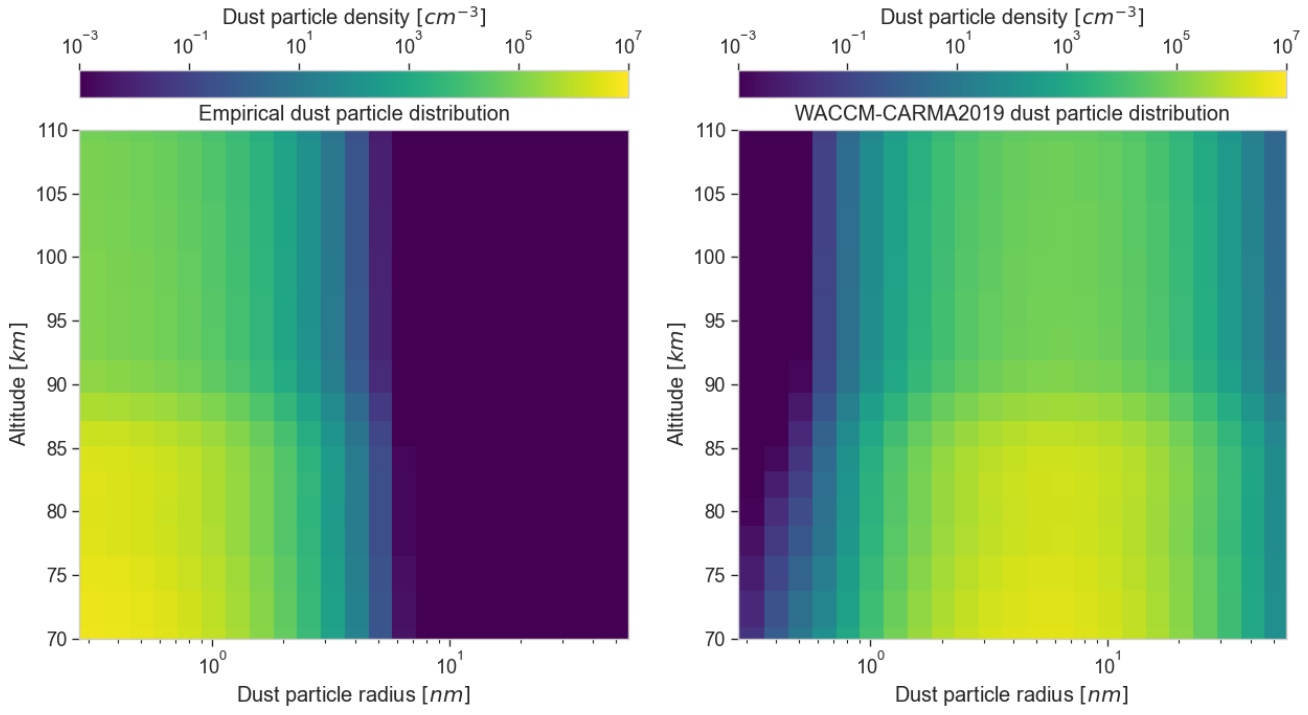


Figure 2. Size distribution of dust particles with respect to the dust particle radius and the altitude according to (left) the empirical model introduced used by Rapp and Thomas (2006) given by Equation (15) and (right) the WACCM/CARMA2019 model. Note that the color scale is the same between the two plots.

time period of 100 s with a time step of 10^{-5} s during the first 10^{-3} s and a time step of 10^{-4} s afterwards ensuring convergence. We found that using 1000 s time period which is of the order of ionospheric variations did not significantly affect the results. To further support this choice, we note that the time constants for photo detachment, photo ionization and electron attachment are shorter than 100s for the case of iron-oxide composition (Rapp, 2009).

2.4 Model limitations

A general limitation of this modeling framework is the uncertainty associated with the parameters used in the charging calculations. Furthermore, the calculations do not account for spatial and temporal variations in the ionosphere, which we assume to be constant in order to isolate the influence of the dust parameters. The different particle-size distributions considered above also represent an additional simplification. Finally, the validity of the model assumptions is limited for small particle sizes.

The charging parameters and optical constants used in this study are assumed to be valid for small solid particles whose properties can be approximated using bulk-material values. This approximation is expected to remain reasonable as long as

https://doi.org/10.5194/egusphere-2026-6504
Preprint. Discussion started: 23 November 2026
© Author(s) 2026. CC BY 4.0 License.

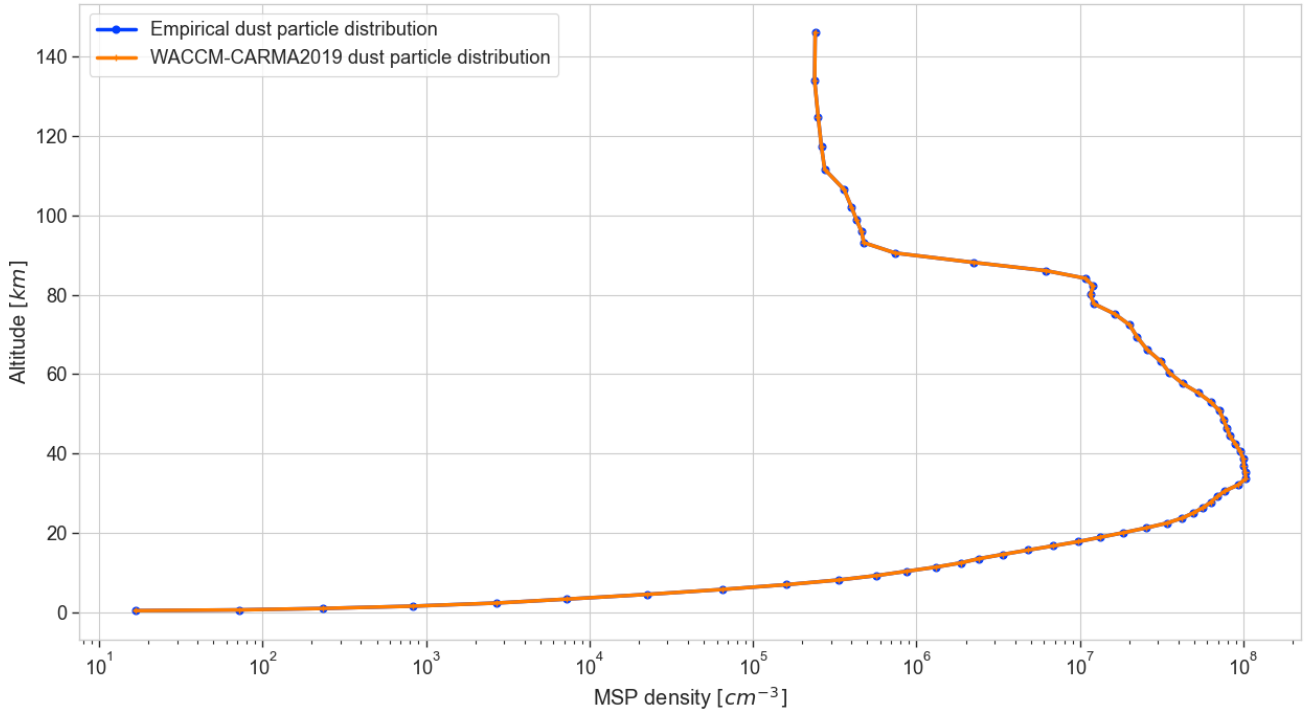


Figure 3. Total radial-integrated dust particle density with respect to the altitude for the empirical and WACCM-CARMA2019 models.

most atoms and molecules are located within the particle rather than at its surface. We assume that this approximation remains valid down to a minimum particle radius of 0.8 nm. Based on a simple estimate for a spherical particle with a bulk density of 2 $\mathrm{g \cdot cm^{-3}}$, such a particle would have a mass of approximately 2500 atomic mass units. Thus, the particle would still consist of a considerable number of atoms or molecules, suggesting that a bulk-material description may remain a reasonable approximation. Rapp (2009) assumes a limit of 1 nm.

We can further assess whether the calculated charges violate the field-emission limits. Very strong electric fields can cause electrons to tunnel out of tiny negatively charged grains, limiting their maximum negative charge to approximately $Z > -\left(1 + 0.7 a_{\mathrm{nm}}^2\right)$ where (a_{nm}) is the grain radius in nanometers (Mann et al., 2014). This would correspond to a grain radius of 1.2 nm for charge state -2. The calculations below show that the number densities of charge state -2 are absent or smaller by 10^2 or more compared to the other charge states. The limiting radius is < 0.2 nm for charge state -1 which is outside the interval of considered sizes. The field emission does not affect positive charge states for the sizes considered in this study because ion emission is by far less likely.

https://doi.org/10.5194/egusphere-2026-6504
Preprint. Discussion started: 23 November 2026
© Author(s) 2026. CC BY 4.0 License.

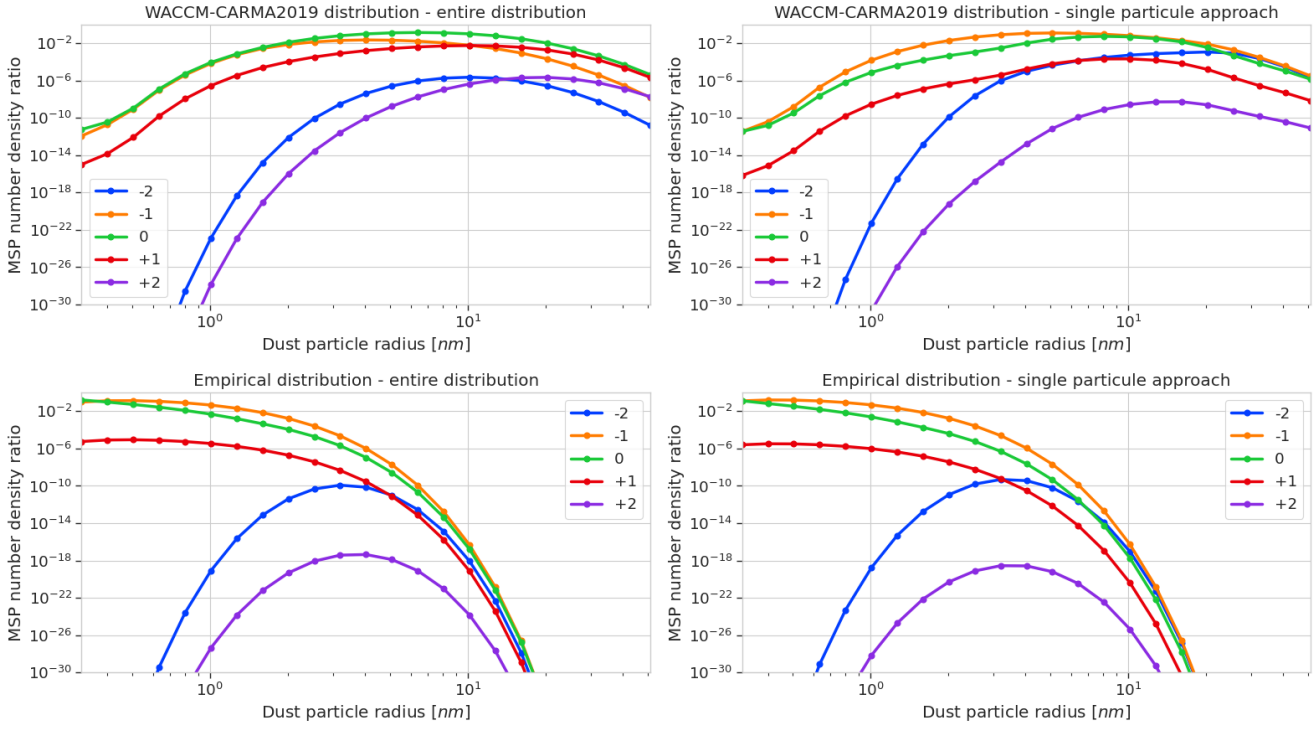


Figure 4. MSP number density with respect to the dust particle radius for different ionization states, namely $-2 \leq Z \leq 2$, and different MSP distribution models when $n_e = n_i = 10 n_{MSP}$.

	Dust particle number density ratio $n_{MSP}(Z)/n_{\text{tot}}$				
	$Z=-2$	$Z=-1$	$Z=0$	$Z=+1$	$Z=+2$
WACCM-CARMA2019 - single particle	5.112×10^{-3}	7.485×10^{-1}	2.455×10^{-1}	8.960×10^{-4}	1.766×10^{-8}
WACCM-CARMA2019 - entire distribution	8.507×10^{-6}	1.280×10^{-1}	8.393×10^{-1}	3.262×10^{-2}	8.247×10^{-6}
Empirical distribution - single particle	1.084×10^{-9}	7.414×10^{-1}	2.586×10^{-1}	1.486×10^{-5}	6.944×10^{-19}
Empirical distribution - entire distribution	2.531×10^{-10}	6.410×10^{-1}	3.589×10^{-1}	4.241×10^{-5}	1.043×10^{-17}

Table 2. Dust particle number density ratio $n_{MSP}(Z)/n_{tot} = \int_{r_{min}}^{r_{max}} n_{MSP}(Z,r)/n_{tot}\, dr$ associated with Figure 4, i.e. when $n_e = n_i = 10 n_{MSP}$.

3 Results and discussion

3.1 The influence of the size distribution

To discuss how the results depend on the size distribution we considering MSP with the parameters for hematite composition at an altitude of 90 km and MSP number densities of the same order as the electron densities. Figure 4 shows the charge

https://doi.org/10.5194/egusphere-2026-6504
Preprint. Discussion started: 23 November 2026
© Author(s) 2026. CC BY 4.0 License.

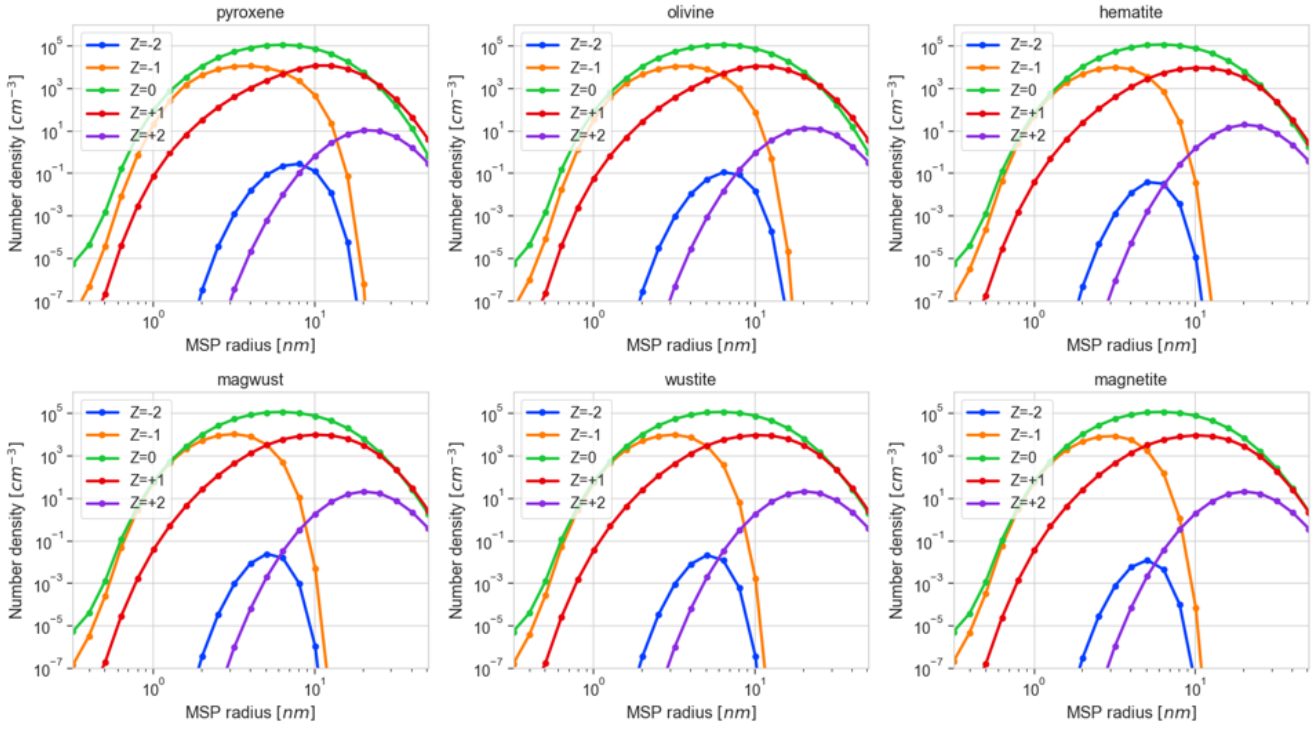


Figure 5. MSP radius distribution for different ionization state, namely $-2 \leq Z \leq 2$, for different compositions.

distribution with respect to the dust particles radius for ionization states $-2 \leq Z \leq 2$ for the empirical distribution and the WACCM-CARMA2019. The results are summarized in Table 2. The major difference between the curves comes from the differences between the size distributions. We now consider what the results imply on the importance of collective effects imposed by the size distribution. Equations (5)-(1) show that charging processes for dust particles with different radii are independent for each dust particle size, but there is a coupling in Equations (11)-(12). Because the rates of the charging process given by Equations (6), (7), (8), and (10) depend on the dust particle radius, an electron or an ion are actually more likely to be captured by a larger particle, and a larger particle is more likely to release a free electron due to photo-ionization or photo-detachment. Individual simulations have been performed by considering one dust particle radius at the time, for which the respective density was taken from the WACCM-CARMA2019. By comparing to the calculations where the size distribution is considered, the charge distributions were found to have the same shape. However, a difference by a factor of two was observed for the total number of density of charged dust particles, that is particles with the different ionization states. This difference by factor of two at maximum, is small in comparison to the differences between the two assumed size distributions.

https://doi.org/10.5194/egusphere-2026-6504
Preprint. Discussion started: 23 November 2026
© Author(s) 2026. CC BY 4.0 License.

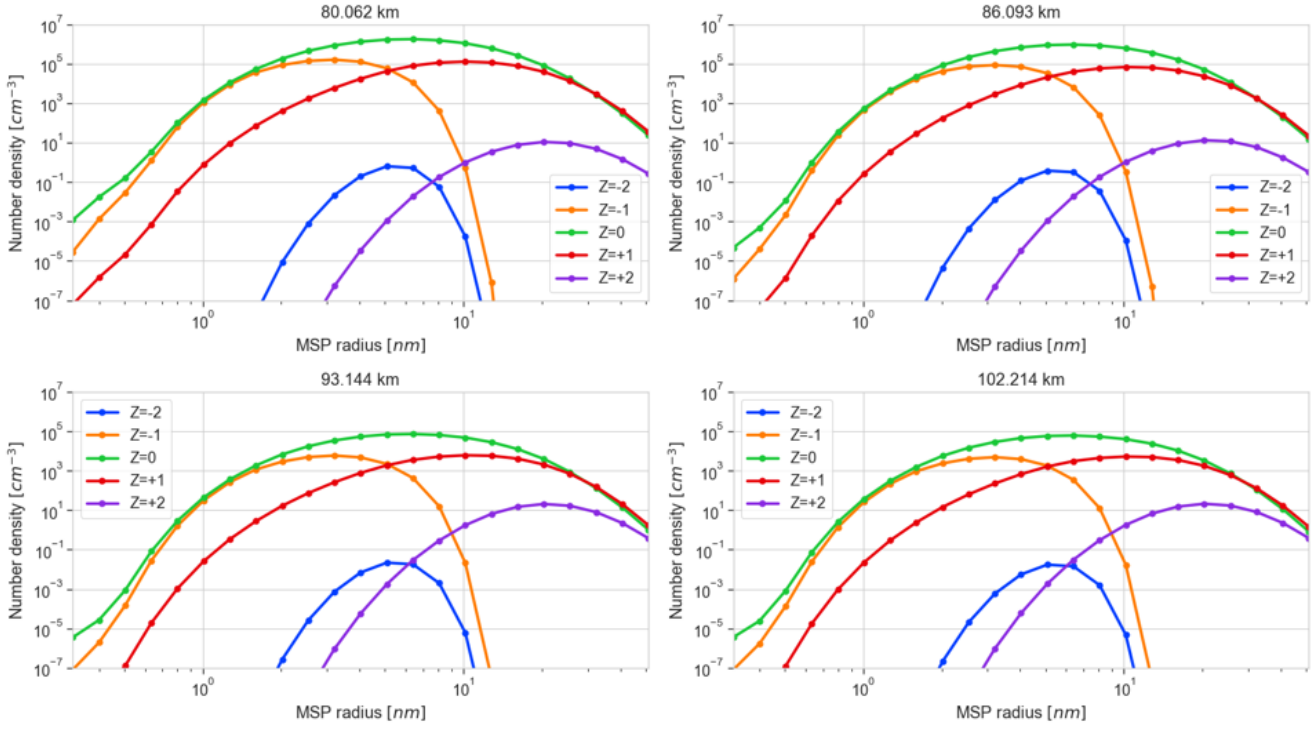


Figure 6. MSP radius distribution for different ionization state, namely $-2 \leq Z \leq 2$, for different altitudes.

3.2 Comparison of MSP compositions

Figure 5 depicts the charge-state distributions as a function of particle size for the different particle compositions considered in this study. Figure 6 depicts this for different heights. The distributions are generally similar for the different MSP compositions. However, the onset of negative charging is shifted toward smaller particle sizes for the silicates—olivine and pyroxene—than for the other materials, which are metal oxides. Nevertheless, even when comparing the silicates with the metal oxides, the effect of composition on the charge-state distributions is small in comparison to size dependence.

Our calculations show that inferring the composition from the charge states alone is difficult in the absence of additional information. The primary factor preventing us from deriving composition information is the the strong effect that the particle size distribution has on the charge densities. In addition, some of the parameters used in the calculations are not sufficiently well known. These include, for example, the optical constants in the ultraviolet range, as well as the work function and electron affinity of some materials. Furthermore, most material parameters are known only for bulk materials, making it difficult to estimate size-dependent effects. The relative importance of the different charge states remains similar except for that the doubly positive charged particles are more abundant with increasing height.

https://doi.org/10.5194/egusphere-2026-6504
Preprint. Discussion started: 23 November 2026
© Author(s) 2026. CC BY 4.0 License.

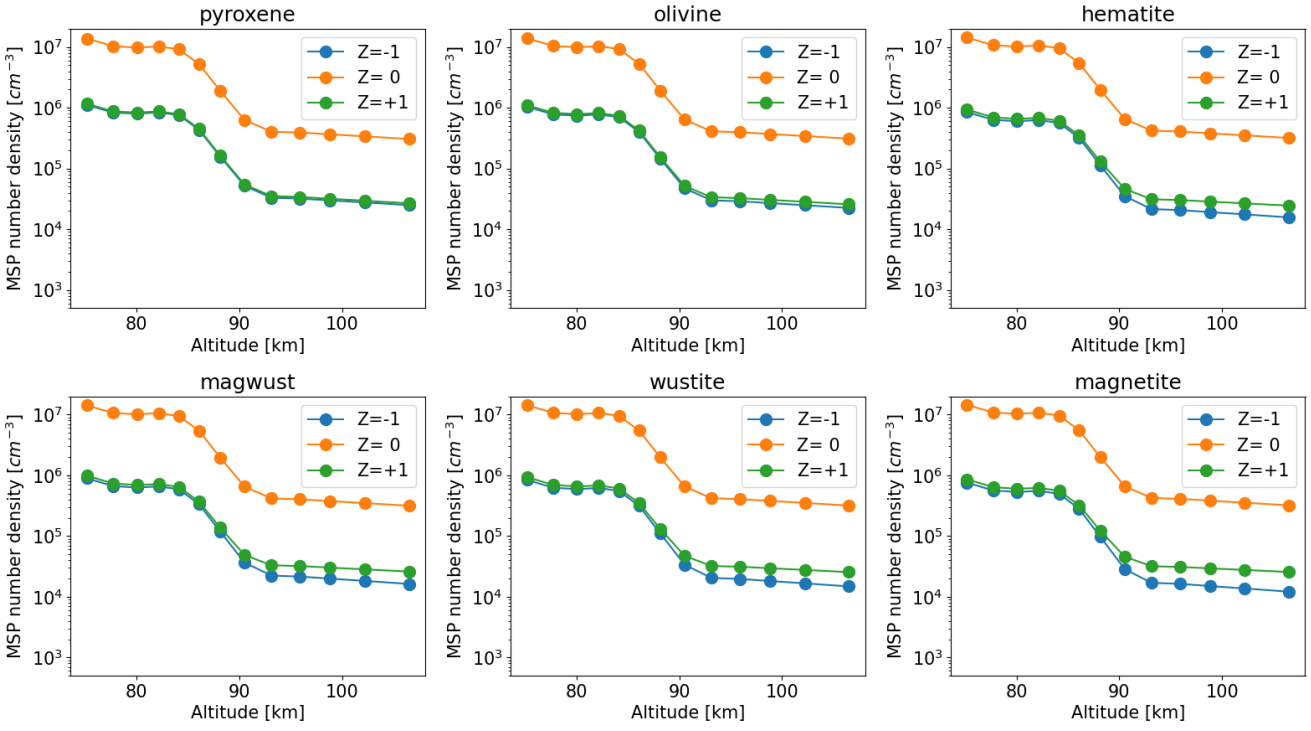


Figure 7. Total MSP number density for different ionization state Z and different MSP compositions. These densities are obtained by summing the MSP distribution over the radius considering MSP larger than 2 nm.

3.3 Height profiles of charged dust

Another important result is that, across the entire altitude range and for all types of material considered, the vast majority of particles are neutral. The height profiles of the integrated charge density are displayed in Figure 7. The charged particles are nearly charge-balanced, with almost equal numbers of positively and negatively charged particles when averaged over the full size distribution. A difference between the two charge polarities becomes noticeable above 90 km for particles larger than 2 nm that are composed of iron oxides. In these cases, the density of positively charged particles is higher. One can also see from the figures that the sharp decrease in charge density with increasing altitude between 80 and 90 km is mainly due to the reduced number density, which decreases by a factor of 15 between 80 and 90 km altitude. This result has implications for the in-situ detection of MSP with instruments on sounding rockets.

There are several different instrument concepts to detect dust in the mesosphere from sounding rockets (Havnes et al., 1996; Gelinas et al., 1998; Lynch et al., 2005; Robertson et al., 2009; Rapp et al., 2012). Dust measurements on sounding rockets are partly based on charged particles striking the detector as the payload moves through the atmosphere. These instruments include different concepts to separate charge polarities or to charge neutral dust particles through different processes. Moreover, the

https://doi.org/10.5194/egusphere-2026-6504
Preprint. Discussion started: 23 November 2026
© Author(s) 2026. CC BY 4.0 License.

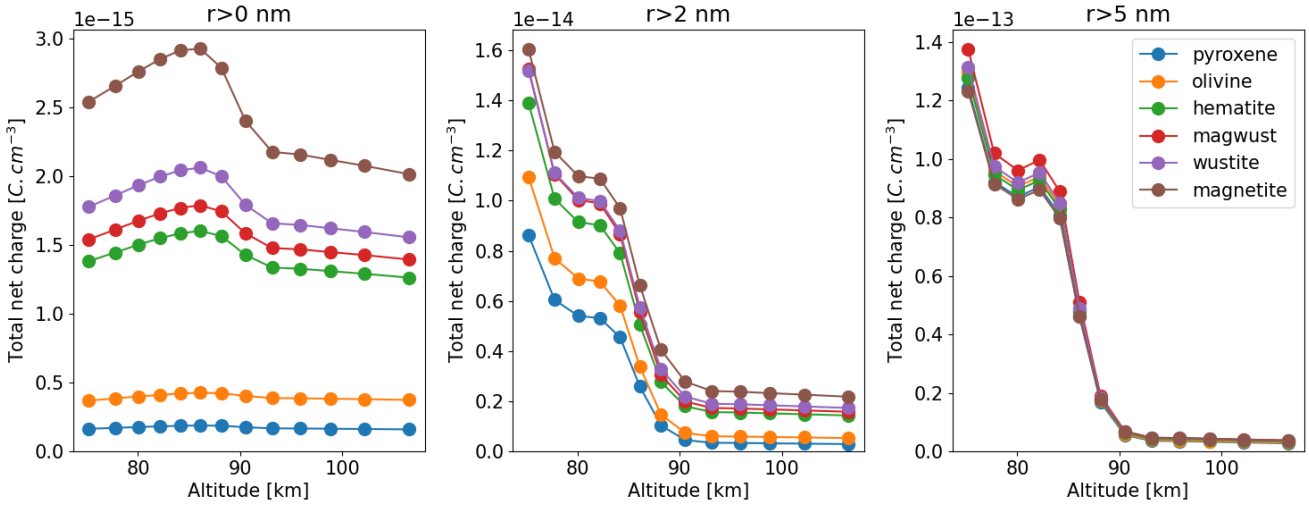


Figure 8. Total charge density as function of height given by Eq. (14).

impact process may generate additional charges (Antonsen et al., 2020). The charge density profiles displayed in Figure (8) indicate the currents generated by the dust surface charges depends on the size range of particles that enter the detector. The current is higher when only a fraction of sizes reaches the detector. Typically larger MSP reach the detector and smaller ones are deflected in the airflow (Havnes et al., 2014). To estimate the direct current generated, we integrate over all charge polarities and obtain:

$$I(z) = A_M v_r \sum_{Z=-1}^{1} \sum_{r=r_{min}}^{r_{max}} Zen_{MSP}(r,Z,z) \tag{16}$$

where A_M is the effective collection area of the detector, v_r is the rocket velocity and all other parameters are as above. To illustrate the charge current we assume the parameters for the Maxidusty campaigns and the dust detector MUDD (Havnes et al., 2014): V_R is assumed to be constant with height at 708 m/s and $AD = 1.2 \times 10^3 m^2$. Additionally, the secondary electrons produced inside the detector are assumed to be negligible. The hence derived currents have altitude profiles that differ from the charge densities displayed in Figure 8 by a constant factor. When assuming $r_{min} = 2nm$ the current found in the 80 to 90 km height interval ranges from roughly $1 - 10nA$, which is in line with experimental data.

4 Conclusions

We investigated the charging of dust particles, MSP in the mesosphere. We calculate the charge states of solid particles a few nanometers in size, taking into account their interactions with photons, atmospheric electrons, and ions. In particular, we investigate the effects of particle composition and size distribution on the charging behavior. We consider both an empirical

https://doi.org/10.5194/egusphere-2026-6504
Preprint. Discussion started: 23 November 2026
© Author(s) 2026. CC BY 4.0 License.

inverse-power-law size distribution and a Gaussian size distribution, centered at a few nanometers, derived from a WACCM/-CARMA model simulation of the spatial distribution and growth of MSPs within the global atmospheric circulation system.

We find that positively and negatively charged particles coexist and are often present in comparable abundances. Positive charge states become more abundant toward the larger-size end of the considered range, whereas negative charge states are more abundant among the smallest particles, with radii of a fraction of a nanometer. Our calculations cover the full range of WACCM/CARMA size intervals for MSPs, corresponding to particle radii of approximately 0.2–50 nm. However, our description of the charging interactions assumes solid particles, and we therefore infer that it is applicable only down to radii of approximately 0.8 nm.

The model results show that the vast majority of subnanometer particles are neutral, although a small fraction of negatively charged particles persists even at the smallest sizes considered. Although the charging network includes charge states up to triply positive and triply negative, the abundance of particles with charges greater than ± 2 is negligible and not presented here.

We investigated how dust composition affects the charge balance through the material dependence of optical constants and find that the total charge density of MSP in the mesosphere may vary by about factor 4 within the different relevant materials that we assumed. The charge density is small for pyroxene and olivine and highest for magnetite. This variation is, however less than the variation in total number density of order of 10 within the 80 to 90 km heights. An implication for in situ measurements with dust detectors is that the detected currents depend critically on the size range of particles entering the instrument

Data availability. All data produced in this study are presented in the manuscript.

Author contributions. I.M., A.P. and I.N.conceived and designed the study. I.N.. and A.L. collected the dust parameters, I.N. made single particle calculations and the light scattering calculations. A.L. provided information on light scattering properties and optical constants, A.P. set up the framework to calculate charging over the size distribution. W.F. provided the WACCM/CARMA model run. H.G. derived the MSP size distribution from the WACCM/CARMA data. YY made the estimates for instrument currents. All authors contributed to the interpretation of the results, critically revised the manuscript for important intellectual content, approved the final version. IM supervised the master thesis projects of I.N. and H.G. and acquired funding for this work.

Competing interests. One of the authors is a member of the editorial board of Annales Geophysicae.

Acknowledgements. This work was supported by the Research Council of Norway through grant numbers NFR 275503 and NFR 240065. The publication charges for this article have been funded by a grant from the publication fund of UiT The Arctic University of Norway. Language and grammar were edited with the assistance of ChatUiT, the official custom-built artificial intelligence chatbot provided by UiT

https://doi.org/10.5194/egusphere-2026-6504
Preprint. Discussion started: 23 November 2026
© Author(s) 2026. CC BY 4.0 License.



The Arctic University of Norway. All the refractive indices used by were sourced from the Database of Optical Constants for Cosmic Dust by the Laboratory Astrophysics Group of AIU Jena.

Appendix A: Appendix

A1 Radial distribution of MSP number density for different electron densities

A2 Total MSP charge states for different compositions and size ranges.

https://doi.org/10.5194/egusphere-2026-6504
Preprint. Discussion started: 23 November 2026
© Author(s) 2026. CC BY 4.0 License.

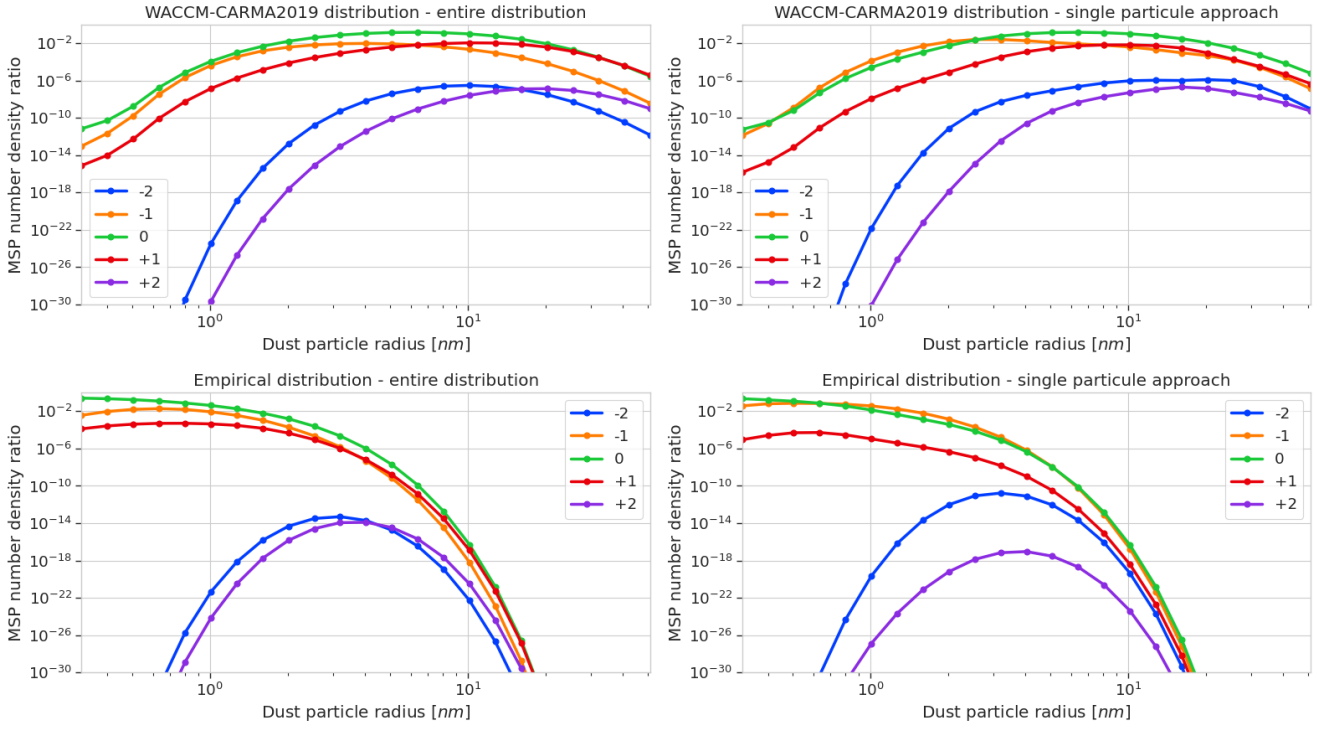


Figure A1. MSP number density with respect to the dust particle radius for different ionization states, namely $-2 \leq Z \leq 2$, and different MSP distribution models when $n_e = n_i = 0.1 n_{MSP}$.

	Dust particle number density ratio $n_{MSP}(Z)/n_{\text{tot}}$				
	$Z=-2$	$Z=-1$	$Z=0$	$Z=+1$	$Z=+2$
WACCM-CARMA2019 - single particle	6.547×10^{-6}	1.269×10^{-1}	8.398×10^{-1}	3.331×10^{-2}	6.253×10^{-7}
WACCM-CARMA2019 - entire distribution	1.127×10^{-6}	5.425×10^{-2}	8.871×10^{-1}	5.863×10^{-2}	5.034×10^{-7}
Empirical distribution - single particle	3.557×10^{-11}	3.616×10^{-1}	6.383×10^{-1}	1.833×10^{-4}	2.052×10^{-17}
Empirical distribution - entire distribution	1.086×10^{-13}	7.744×10^{-2}	9.198×10^{-1}	2.784×10^{-3}	3.059×10^{-14}

Table A1. Dust particle number density ratio $n_{MSP}(Z)/n_{tot} = \int_{r_{min}}^{r_{max}} n_{MSP}(Z,r)/n_{tot}\, dr$ associated with Figure **??**, i.e. when $n_e = n_i = 0.1 n_{MSP}$.

https://doi.org/10.5194/egusphere-2026-6504
Preprint. Discussion started: 23 November 2026
© Author(s) 2026. CC BY 4.0 License.

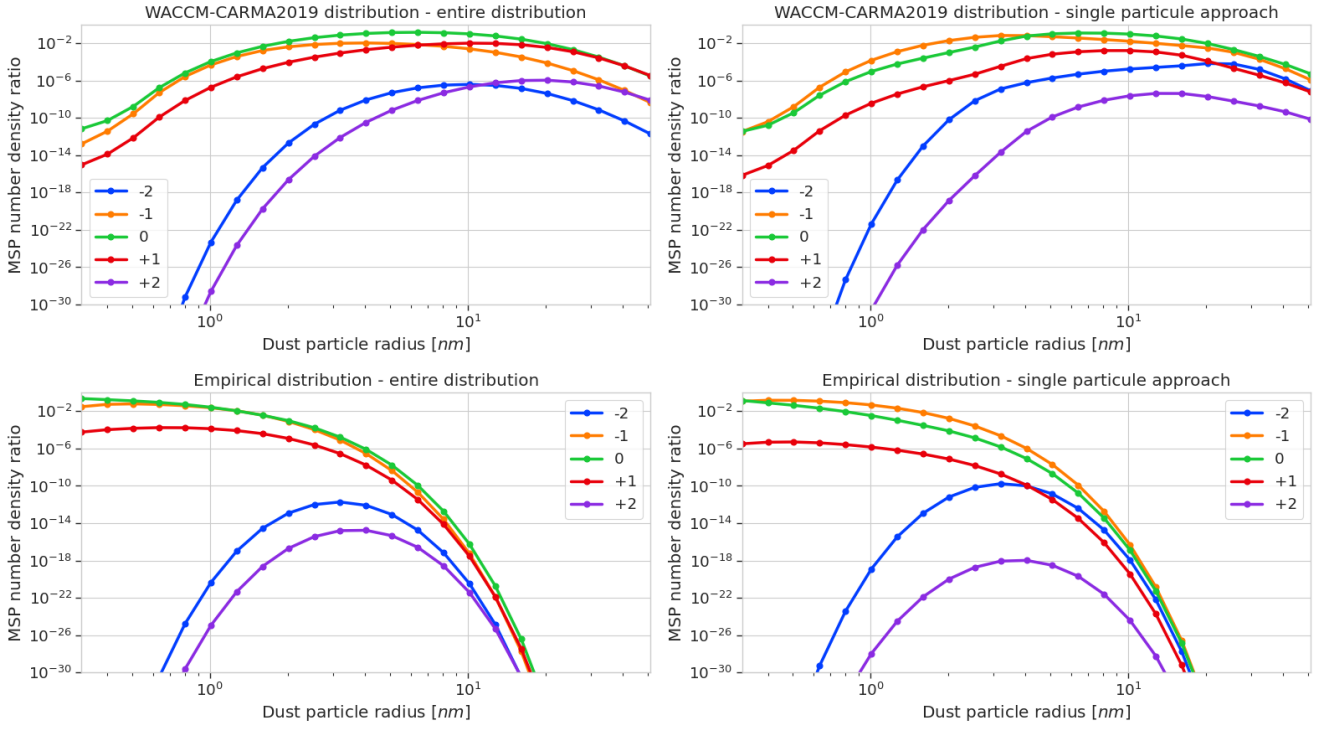


Figure A2. MSP number density with respect to the dust particle radius for different ionization states, namely $-2 \leq Z \leq 2$, and different MSP distribution models when $n_e = n_i = n_{MSP}$.

	Dust particle number density ratio $n_{MSP}(Z)/n_{\text{tot}}$				
	$Z=-2$	$Z=-1$	$Z=0$	$Z=+1$	$Z=+2$
WACCM-CARMA2019 - single particle	2.475×10^{-4}	3.560×10^{-1}	6.364×10^{-1}	7.371×10^{-3}	1.461×10^{-7}
WACCM-CARMA2019 - entire distribution	1.459×10^{-6}	6.073×10^{-2}	8.845×10^{-1}	5.476×10^{-2}	4.039×10^{-6}
Empirical distribution - single particle	3.661×10^{-10}	6.995×10^{-1}	3.005×10^{-1}	2.247×10^{-5}	2.437×10^{-18}
Empirical distribution - entire distribution	3.916×10^{-12}	2.804×10^{-1}	7.186×10^{-1}	9.336×10^{-4}	4.205×10^{-15}

Table A2. Dust particle number density ratio $n_{MSP}(Z)/n_{tot} = \int_{r_{min}}^{r_{max}} n_{MSP}(Z,r)/n_{tot}\, \mathrm{d}r$ associated with Figure A2, i.e. when $n_e = n_i = n_{MSP}$.

https://doi.org/10.5194/egusphere-2026-6504
Preprint. Discussion started: 23 November 2026
© Author(s) 2026. CC BY 4.0 License.

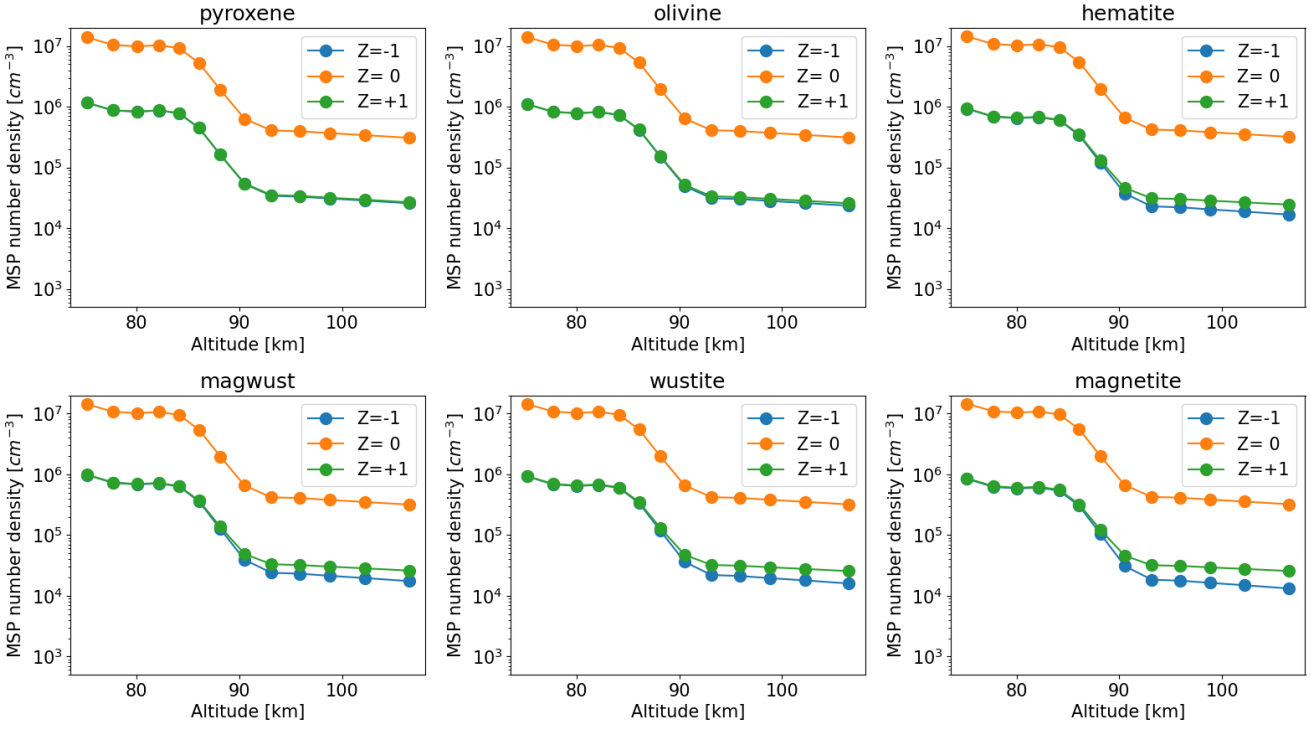


Figure A3. Total MSP number density for different ionization state Z and different MSP compositions. These densities are obtained by summing the MSP distribution over the radius considering MSP larger than 5 nm.

https://doi.org/10.5194/egusphere-2026-6504
Preprint. Discussion started: 23 November 2026
© Author(s) 2026. CC BY 4.0 License.

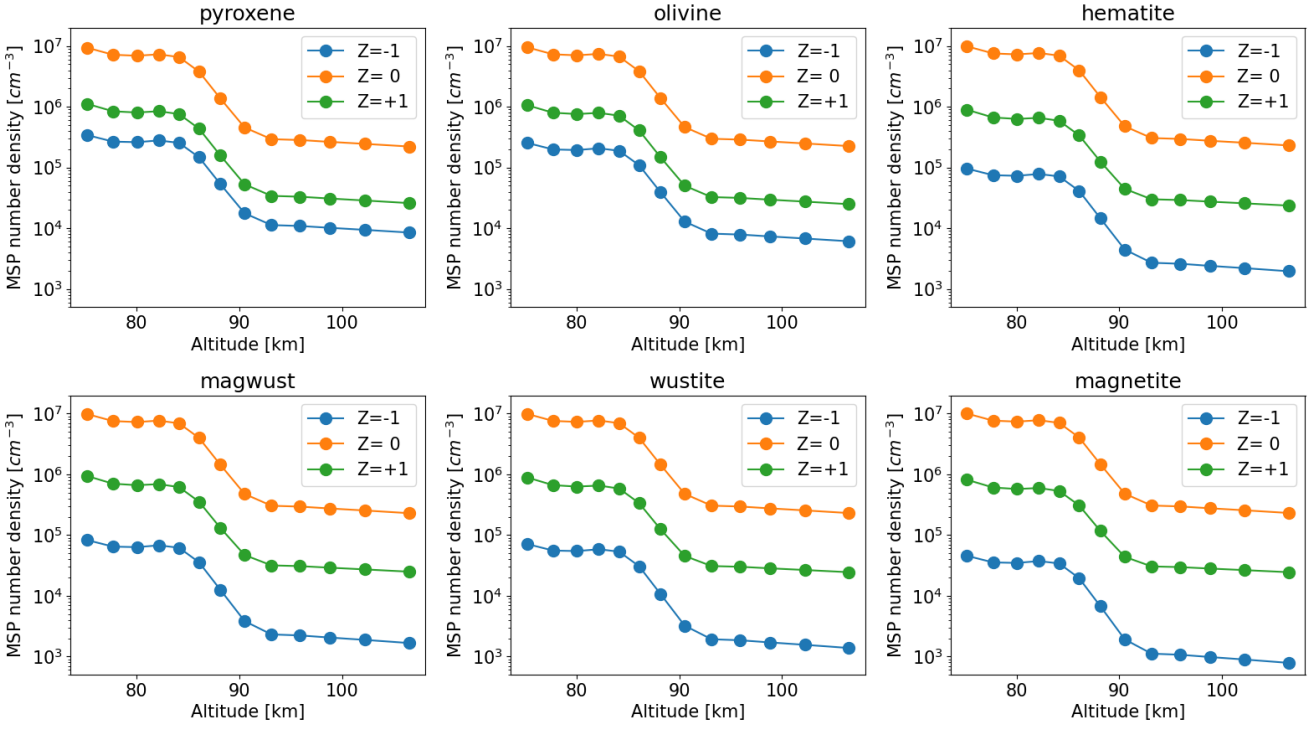


Figure A4. Total MSP number density for different ionization state Z and different MSP compositions. These densities are obtained by summing the MSP distribution over the radius considering all MSP.

https://doi.org/10.5194/egusphere-2026-6504
Preprint. Discussion started: 23 November 2026
© Author(s) 2026. CC BY 4.0 License.

References

Antonsen, T., Havnes, O., and Mann, I.: Estimates of the Size Distribution of Meteoric Smoke Particles From Rocket-Borne Impact Probes, Journal of Geophysical Research: Atmospheres, 122, 2017.

Antonsen, T., Mann, I., Vaverka, J., Nouzak, L., and Fredriksen, Å.: A Comparison of Contact Charging and Impact Ionization in Low Velocity Impacts: Implications for Dust Detection in Space, Annales Geophysicae Discussions, pp. 1–26, 2020.

Asmus, H., Robertson, S., Dickson, S., Friedrich, M., and Megner, L.: Charge balance for the mesosphere with meteoric dust particles, Journal of Atmospheric and Solar-Terrestrial Physics, 127, 137–149, 2015.

Baptiste, J., Williamson, C., Fox, J., Stace, A. J., Hassan, M., Braun, S., Stamm, B., Mann, I., and Besley, E.: The influence of surface charge on the coalescence of ice and dust particles in the mesosphere, Atmospheric Chemistry and Physics Discussions, 2020, 1–16, 2020.

Bardeen, C., Toon, O., Jensen, E., Marsh, D., and Harvey, V.: Numerical simulations of the three-dimensional distribution of meteoric dust in the mesosphere and upper stratosphere, Journal of Geophysical Research: Atmospheres, 113, 2008.

Baumann, C., Rapp, M., Kero, A., and Enell, C.-F.: Meteor smoke influences on the D-region charge balance - review of recent in situ measurements and one-dimensional model results, Annales Geophysicae, 31, 2049–2062, https://doi.org/10.5194/angeo-31-2049-2013, 2013.

Bohren, C. F. and Olivero, J. J.: Evidence for haematite particles at 60 km altitude, Nature, 310, 216–218, 1984.

Dorschner, J., Begemann, B., Henning, T., Jaeger, C., and Mutschke, H.: Steps toward Interstellar Silicate Mineralogy. II. Study of Mg-Fe-silicate Glasses of Variable Composition., Astronomy and Astrophysics, 300, 503, 1995.

Fonin, M., Pentcheva, R., Dedkov, Yu. S., Sperlich, M., Vyalikh, D. V., Scheffler, M., Rüdiger, U., and Güntherodt, G.: Surface Electronic Structure of the Fe 3 O 4 (100) : Evidence of a Half-Metal to Metal Transition, Physical Review B, 72, 104 436, https://doi.org/10.1103/PhysRevB.72.104436, 2005.

Gabrielli, P., Barbante, C., Plane, J. M. C., Varga, A., Hong, S., Cozzi, G., Gaspari, V., Planchon, F. A. M., Cairns, W., Ferrari, C., Crutzen, P., Cescon, P., and Boutron, C. F.: Meteoric smoke fallout over the Holocene epoch revealed by iridium and platinum in Greenland ice, Nature, 432, 1011–1014, 2004.

Gelinas, L. J., Lynch, K. A., Kelley, M., Collins, S., Baker, S., Zhou, Q., and Friedman, J.: First observation of meteoritic charged dust in the tropical mesosphere, Geophysical Research Letters, 25, 4047–4050, 1998.

Greaker, H.: On the Distribution of Meteoric Smoke Particles above Andøya, Norway, and Estimated Collection During a Summer Rocket Campaign, Master thesis, UiT Norges Arktiske Universitet, 2023.

Gumbel, J. and Megner, L.: Charged meteoric smoke as ice nuclei in the mesosphere: Part 1—A review of basic concepts, Journal of Atmospheric and Solar-Terrestrial Physics, 71, 1225–1235, 2009.

Gunnarsdottir, T. L., Mann, I., Feng, W., Huyghebaert, D. R., Haeggstroem, I., Ogawa, Y., Saito, N., Nozawa, S., and Kawahara, T. D.: Influence of Meteoric Smoke Particles on the Incoherent Scatter Measured with EISCAT VH, Annales Geophysicae Discussions, 2023, 1–22, https://doi.org/10.5194/angeo-2023-29, 2023.

Havnes, O., Trøim, J., Blix, T., Mortensen, W., Næsheim, L., Thrane, E., and Tønnesen, T.: First detection of charged dust particles in the Earth's mesosphere, Journal of Geophysical Research: Space Physics, 101, 10 839–10 847, 1996.

Havnes, O., Gumbel, J., Antonsen, T., Hedin, J., and La Hoz, C.: On the size distribution of collision fragments of NLC dust particles and their relevance to meteoric smoke particles, Journal of Atmospheric and Solar-Terrestrial Physics, 118, 190–198, 2014.

He, C.: Work Function of α-Fe_{2}O_{3} : A DFT Calculation, https://doi.org/10.48550/ARXIV.1709.04672, 2017.

https://doi.org/10.5194/egusphere-2026-6504
Preprint. Discussion started: 23 November 2026
© Author(s) 2026. CC BY 4.0 License.

Henning, T., Begemann, B., Mutschke, H., and Dorschner, J.: Optical properties of oxide dust grains., Astronomy and Astrophysics Supplement, v. 112, p. 143, 112, 143, 1995a.

Henning, T., Begemann, B., Mutschke, H., and Dorschner, J.: Optical Properties of Oxide Dust Grains., Astronomy and Astrophysics Supplement Series, 112, 143, 1995b.

Hervig, M., Thompson, R. E., McHugh, M., Gordley, L. L., Russell III, J. M., and Summers, M. E.: First confirmation that water ice is the primary component of polar mesospheric clouds, Geophysical Research Letters, 28, 971–974, 2001.

Hervig, M. E., Deaver, L. E., Bardeen, C. G., Russell III, J. M., Bailey, S. M., and Gordley, L. L.: The content and composition of meteoric smoke in mesospheric ice particles from SOFIE observations, Journal of Atmospheric and Solar-Terrestrial Physics, 84, 1–6, 2012.

Hervig, M. E., Brooke, J. S. A., Feng, W., Bardeen, C. G., and Plane, J. M. C.: Constraints on Meteoric Smoke Composition and Meteoric Influx Using SOFIE Observations With Models, Journal of Geophysical Research: Atmospheres, 122, 13,495–13,505, https://doi.org/https://doi.org/10.1002/2017JD027657, 2017.

Hervig, M. E., Plane, J. M., Siskind, D. E., Feng, W., Bardeen, C. G., and Bailey, S. M.: New global meteoric smoke observations from SOFIE: Insight regarding chemical composition, meteoric influx, and hemispheric asymmetry, Journal of Geophysical Research: Atmospheres, 126, e2021JD035 007, 2021.

Hunten, D. M., Turco, R. P., and Toon, O. B.: Smoke and Dust Particles of Meteoric Origin in the Mesosphere and Stratosphere, Journal of Atmospheric Sciences, 37, 1342 – 1357, 1980.

Jaeger, C., Mutschke, H., Begemann, B., Dorschner, J., and Henning, Th.: Steps toward Interstellar Silicate Mineralogy. I. Laboratory Results of a Silicate Glass of Mean Cosmic Composition., Astronomy and Astrophysics, 292, 641–655, 1994.

Jäger, C., Mutschke, H., Begemann, B., Dorschner, J., and Henning, T.: Steps toward interstellar silicate mineralogy. 1: Laboratory results of a silicate glass of mean cosmic composition, Astronomy and Astrophysics (ISSN 0004-6361), vol. 292, no. 2, p. 641-655, 292, 641–655, 1994.

Knappmiller, S., Rapp, M., Robertson, S., and Gumbel, J.: Charging of meteoric smoke and ice particles in the mesosphere including photoemission and photodetachment rates, Journal of atmospheric and solar-terrestrial physics, 73, 2212–2220, 2011.

Kraushofer, F., Jakub, Z., Bichler, M., Hulva, J., Drmota, P., Weinold, M., Schmid, M., Setvin, M., Diebold, U., Blaha, P., and Parkinson, G. S.: Atomic-Scale Structure of the Hematite α-Fe $_2$ O $_3$ ($1\bar{1}02$) "R-Cut" Surface, The Journal of Physical Chemistry C, 122, 1657–1669, https://doi.org/10.1021/acs.jpcc.7b10515, 2018.

Li, X. Y., Gan, H., Mo, B., Wang, S. J., Wei, G. F., Tang, H., and Zhao, Y. Y. S.: Indication of Mineral Work Function in Lunar Dust Electrostatic Migration, p. 1993, 2016.

Luebken, F.-J., Baumgarten, G., Grygylashvyly, M., and Vellalassery, A.: Absorption of solar radiation by noctilucent clouds in a changing climate, 2023.

Lynch, K. A., Gelinas, L. J., Kelley, M., Collins, R., Widholm, M., Rau, D., MacDonald, E., Liu, Y., Ulwick, J., and Mace, P.: Multiple sounding rocket observations of charged dust in the polar winter mesosphere, Journal of Geophysical Research: Space Physics, 110, 2005.

Mann, I., Meyer-Vernet, N., and Czechowski, A.: Dust in the planetary system: Dust interactions in space plasmas of the solar system, Physics reports, 536, 1–39, 2014.

Megner, L. and Gumbel, J.: Charged meteoric particles as ice nuclei in the mesosphere: Part 2: A feasibility study, Journal of Atmospheric and Solar-Terrestrial Physics, 71, 1236–1244, 2009.

Megner, L., Gumbel, J., Rapp, M., and Siskind, D.: Reduced meteoric smoke particle density at the summer pole–Implications for mesospheric ice particle nucleation, Advances in space research, 41, 41–49, 2008a.

https://doi.org/10.5194/egusphere-2026-6504
Preprint. Discussion started: 23 November 2026
© Author(s) 2026. CC BY 4.0 License.

Megner, L., Siskind, D., Rapp, M., and Gumbel, J.: Global and temporal distribution of meteoric smoke: A two-dimensional simulation study, Journal of Geophysical Research: Atmospheres, 113, 2008b.

Murphy, D. M., Abou-Ghanem, M., Cziczo, D. J., Froyd, K. D., Jacquot, J., Lawler, M. J., Maloney, C., Plane, J. M., Ross, M. N., Schill, G. P., et al.: Metals from spacecraft reentry in stratospheric aerosol particles, Proceedings of the National Academy of Sciences, 120, e2313374 120, 2023.

Natanson, G.: On the theory of the charging of amicroscopic aerosol particles as a result of capture of gas ions, Sov. Phys. Tech. Phys., 30, 573–588, 1960.

Nerland, I.: Investigation into the photon interaction of small mesospheric dust and its impact on the ionospheric charge balance, Master's thesis UiT Arctic University of Norway, https://hdl.handle.net/10037/34024, 2024.

Plane, J. M., Feng, W., and Dawkins, E. C.: The mesosphere and metals: Chemistry and changes, Chemical reviews, 115, 4497–4541, 2015.

Rapp, M.: Capture rates of electrons and positive ions by mesospheric aerosol particles, Journal of Aerosol Science, 31, 1367–1369, 2000.

Rapp, M.: Charging of mesospheric aerosol particles: the role of photodetachment and photoionization from meteoric smoke and ice particles, in: Annales Geophysicae, vol. 27, pp. 2417–2422, Copernicus Publications Göttingen, Germany, 2009.

Rapp, M. and Thomas, G. E.: Modeling the microphysics of mesospheric ice particles: Assessment of current capabilities and basic sensitivities, Journal of Atmospheric and Solar-Terrestrial Physics, 68, 715–744, 2006.

Rapp, M., Strelnikova, I., Strelnikov, B., Hoffmann, P., Friedrich, M., Gumbel, J., Megner, L., Hoppe, U.-P., Robertson, S., Knappmiller, S., et al.: Rocket-borne in situ measurements of meteor smoke: Charging properties and implications for seasonal variation, Journal of Geophysical Research: Atmospheres, 115, 2010.

Rapp, M., Plane, J. M. C., Strelnikov, B., Stober, G., Ernst, S., Hedin, J., Friedrich, M., and Hoppe, U.-P.: In situ observations of meteor smoke particles (MSP) during the Geminids 2010: constraints on MSP size, work function and composition, Annales Geophysicae, 30, 1661–1673, 2012.

Richter, J. H., Sassi, F., Garcia, R. R., Matthes, K., and Fischer, C. A.: Dynamics of the middle atmosphere as simulated by the Whole Atmosphere Community Climate Model, version 3 (WACCM3), Journal of Geophysical Research: Atmospheres, 113, 2008.

Rienstra-Kiracofe, J. C., Tschumper, G. S., Schaefer, H. F., Nandi, S., and Ellison, G. B.: Atomic and Molecular Electron Affinities: Photoelectron Experiments and Theoretical Computations, Chemical Reviews, 102, 231–282, https://doi.org/10.1021/cr990044u, from table 10., 2002.

Robertson, S., Horányi, M., Knappmiller, S., Sternovsky, Z., Holzworth, R. H., Shimogawa, M. M., Friedrich, M., Torkar, K., Gumbel, J., Megner, L., et al.: Mass analysis of charged aerosol particles in NLC and PMSE during the ECOMA/MASS campaign, 2009.

Sana, T., Mishra, S. K., and Mann, I.: Electrostatics and Collision Dynamics of Ice and Anthropogenic Smoke Particles in the Mesosphere/Lower Thermosphere, EGUsphere, 2026, 1–26, 2026.

Saunders, R. W. and Plane, J. M.: A laboratory study of meteor smoke analogues: Composition, optical properties and growth kinetics, Journal of Atmospheric and Solar-Terrestrial Physics, 68, 2182–2202, 2006.

Schulz, L., Glassmeier, K.-H., Herberhold, M., Mitchell, A., Murphy, D. M., Plane, J. M., and Plaschke, F.: Space waste: An update of the anthropogenic matter injection into Earth's atmosphere, Advances in Space Research, 2026.

Tanaka, K. K., Mann, I., and Kimura, Y.: Formation of ice particles through nucleation in the mesosphere, Atmospheric Chemistry and Physics, 22, 5639–5650, 2022.

Toon, O. B., Turco, R., Hamill, P., Kiang, C., and Whitten, R.: A one-dimensional model describing aerosol formation and evolution in the stratosphere: II. Sensitivity studies and comparison with observations, J. atmos. Sci, 36, 718–736, 1979.

https://doi.org/10.5194/egusphere-2026-6504
Preprint. Discussion started: 23 November 2026
© Author(s) 2026. CC BY 4.0 License.



Turco, R., Hamill, P., Toon, O., Whitten, R., and Kiang, C.: A one-dimensional model describing aerosol formation and evolution in the stratosphere: I. Physical processes and mathematical analogs, Journal of Atmospheric Sciences, 36, 699–717, 1979.

Wang, L.-S., Wu, H., and Desai, S. R.: Sequential Oxygen Atom Chemisorption on Surfaces of Small Iron Clusters, Physical Review Letters, 76, 4853–4856, https://doi.org/10.1103/PhysRevLett.76.4853, interpreted from fig. 2., 1996.